Crustal and Upper Mantle Deformation Beneath Northwestern part of North Anatolian Fault Zone from Harmonic Decomposition of Receiver Functions

Derya Keleş[1], Tuna Eken[1], Andrea Licciardi[2], Tuncay Taymaz[1]

[1]*Istanbul Technical University, Faculty of Mines, Department of Geophysical Engineering, Maslak/Istanbul, Turkey*

[2] *Université Côte d'Azur, CNRS, Observatoire de la Côte d'Azur, IRD, Géoazur, Sophia Antipolis, France*

kelesde@itu.edu.tr

EGU Online Conference | 07.05.2020

Content

Introduction

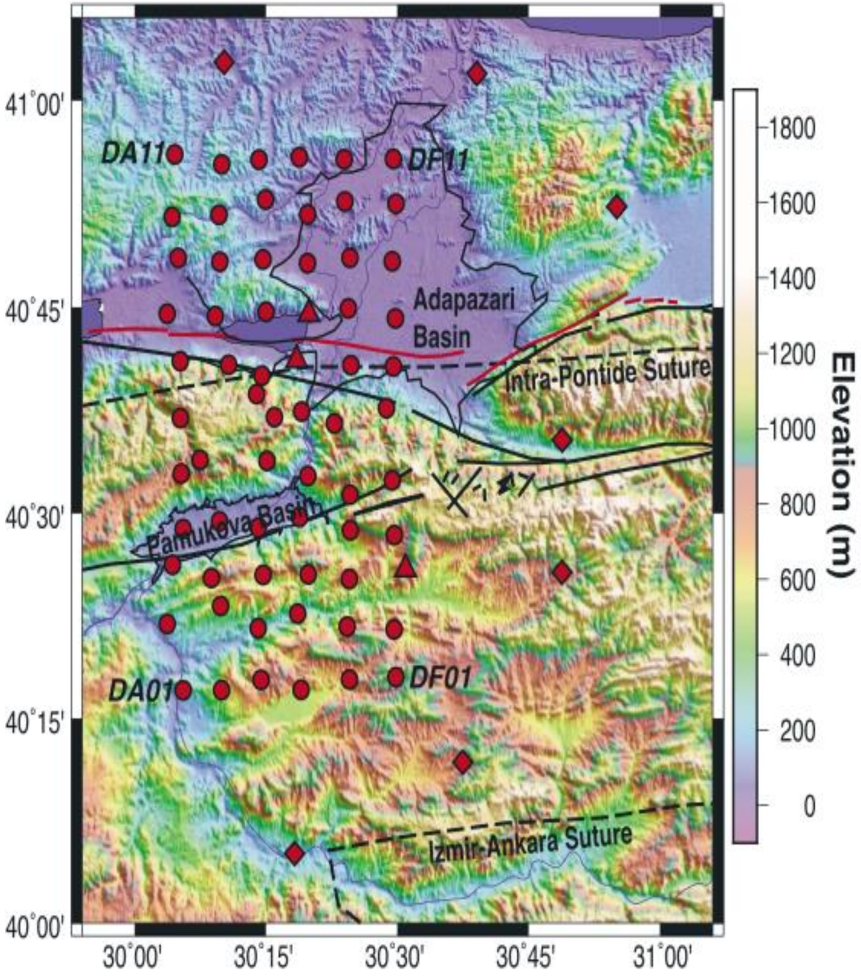

(Frederiksen et al., 2015)

Dense Array for North Anatolia (DANA)

- The dataset is obtained from project was performed by the FaultLab Group in Leeds University
- 72 stations in total
- Examine the anisotropy using the scattering waves beneath the crust and upper mantle around the northwestern (NW) part of North Anatolian Fault Zone (NAFZ)

- Aim of Study
- Understanding the source of seismic anisotropy in the crust
  - LPO or SPO? Which one is dominant in the study area?
- To map the strength and variation of azimuthal anisotropy at varying depths
- The role of the NAFZ on the observed crustal anisotropy signals

Geological Indications

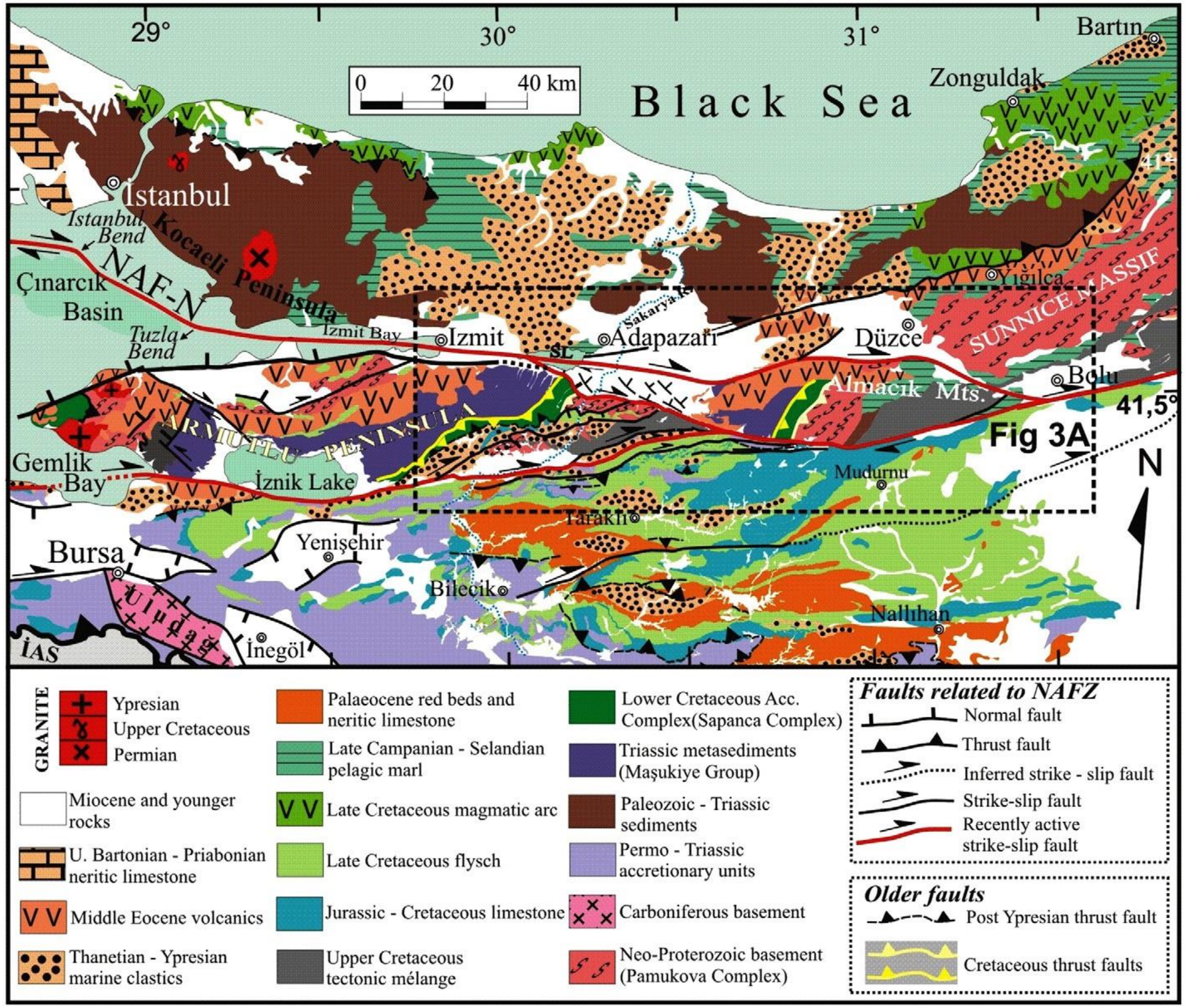

(Akbayram et al., 2016)

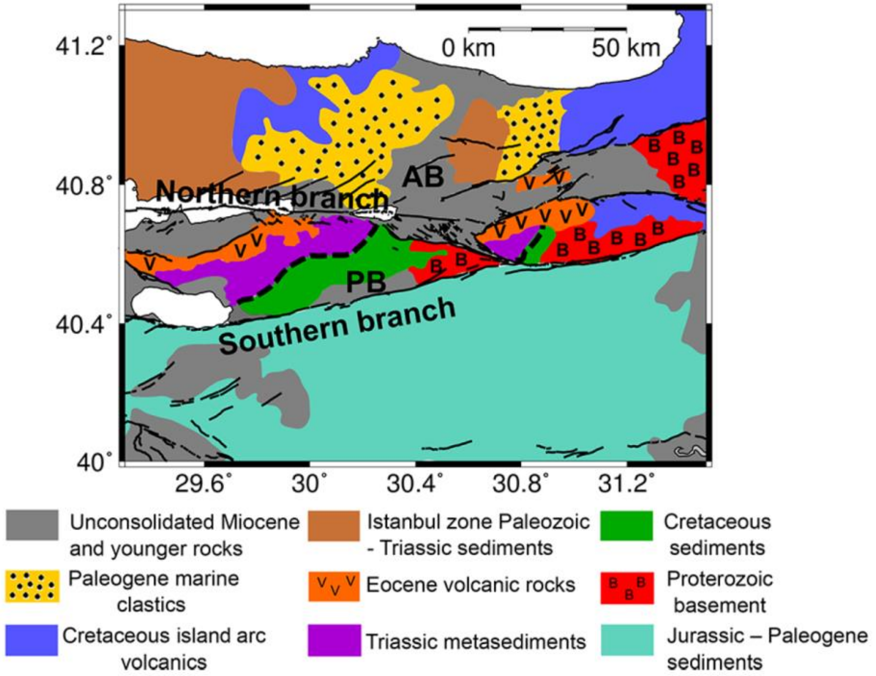

(Taylor et al., 2019)

4 Major Tectonic Regions

- Istanbul-Zonguldak Zone: Mostly comprised by sedimantary rocks above the magmatic basement.
- Armutlu Peninsula: Sediments and Metasediments with Cretaceous and Triassic ages, and Eocene volcanic rocks.
- Almacık Region: Magmatic basement with Proterozoic age and volcanic rocks with Cretaceous age originated from island arc tectonicsm above them
- Sakarya Zone: Mostly consist of Jurassic – Paleogene sediments

Previous Studies - Frederiksen et al. (2015)

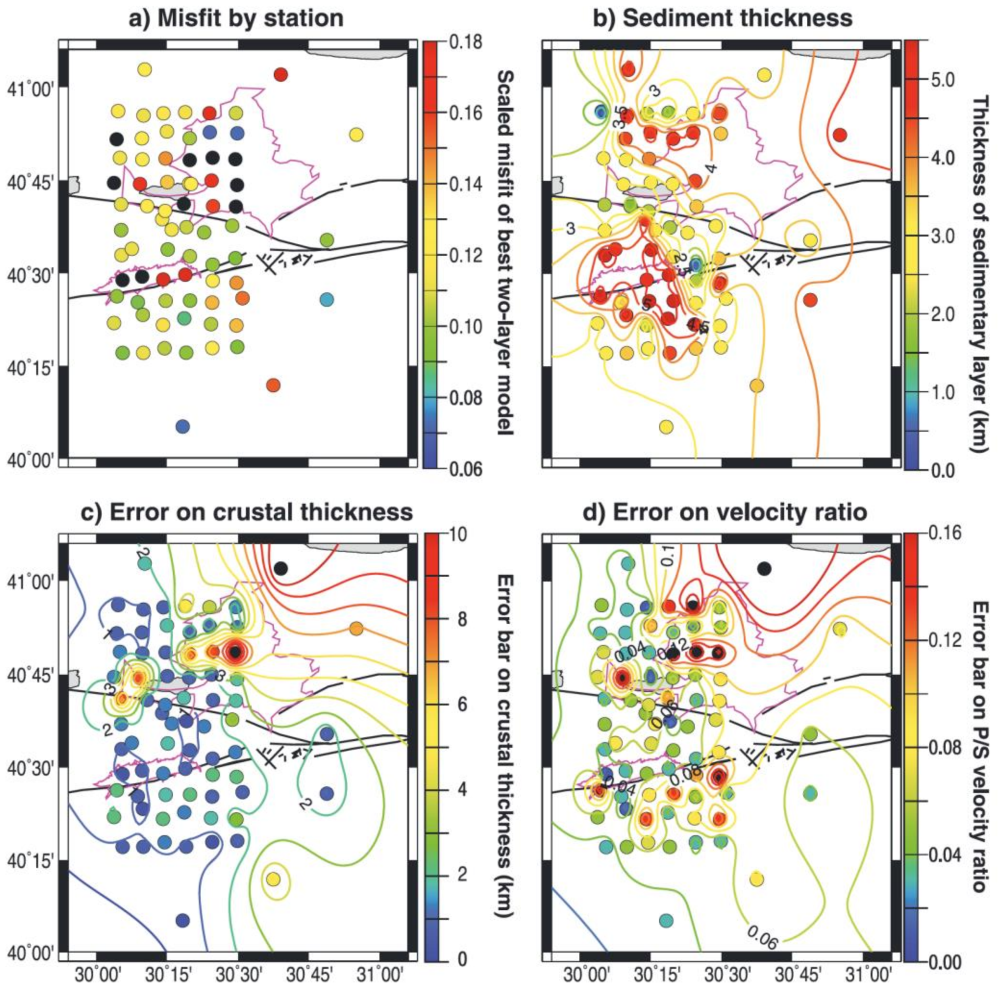

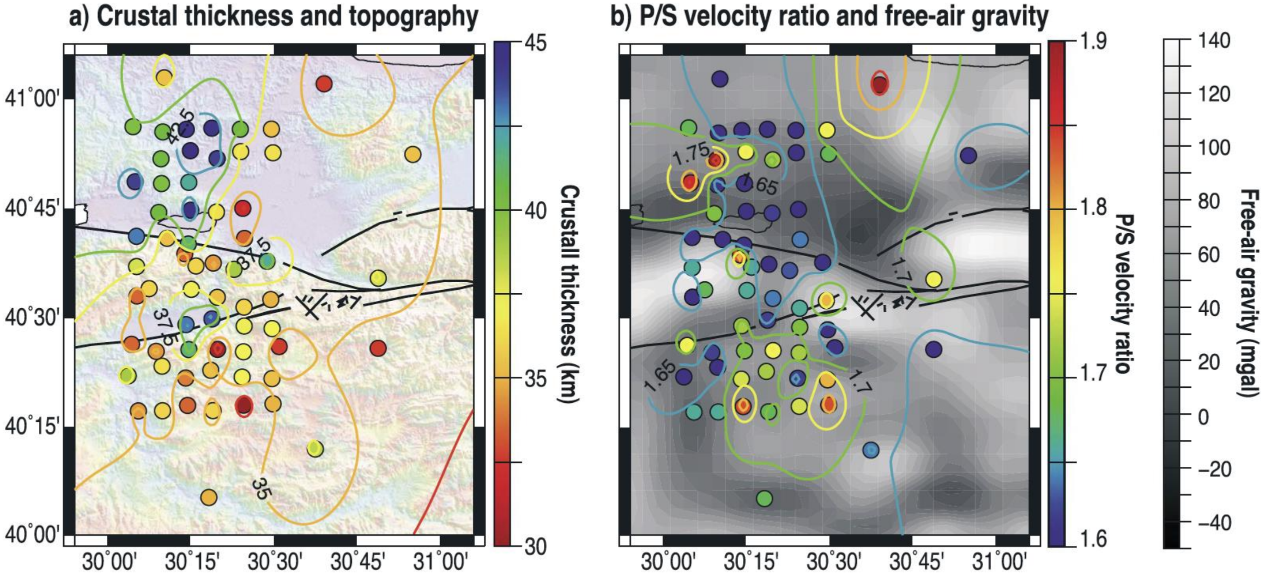

- RFs analyses using transfer function method
- Sedimentary basin thickness: approx. between 1.5 - 5.5 km
- Crustal thickness: varies between 30 – 45 km
- 7 km increasing in Moho boundary from south to north
- Vp/Vs ratio: varies between 1.6 - 1.75

Previous Studies- Kahraman et al. (2015)

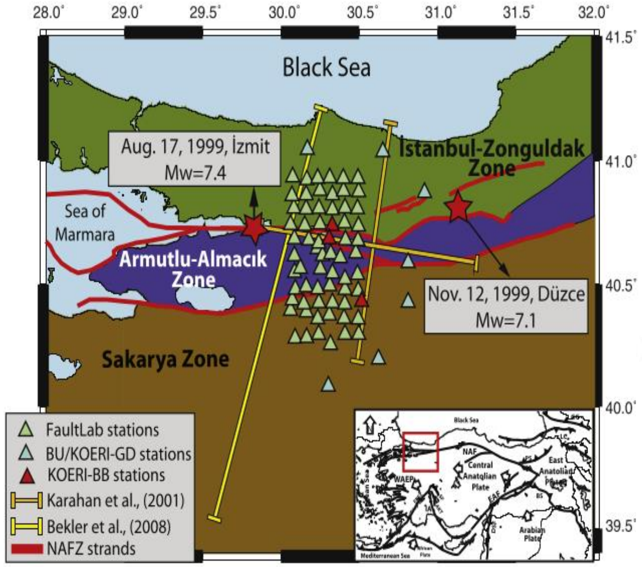

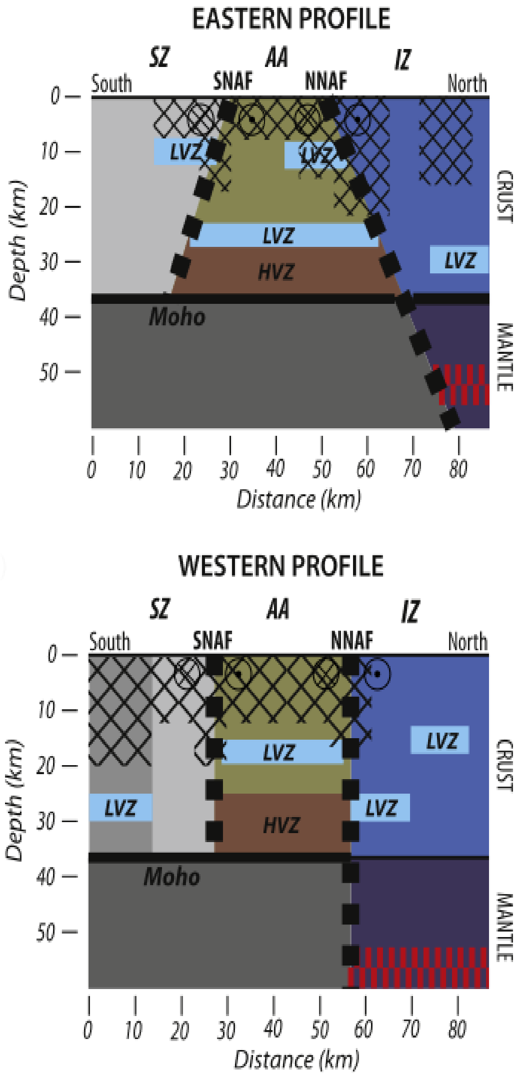

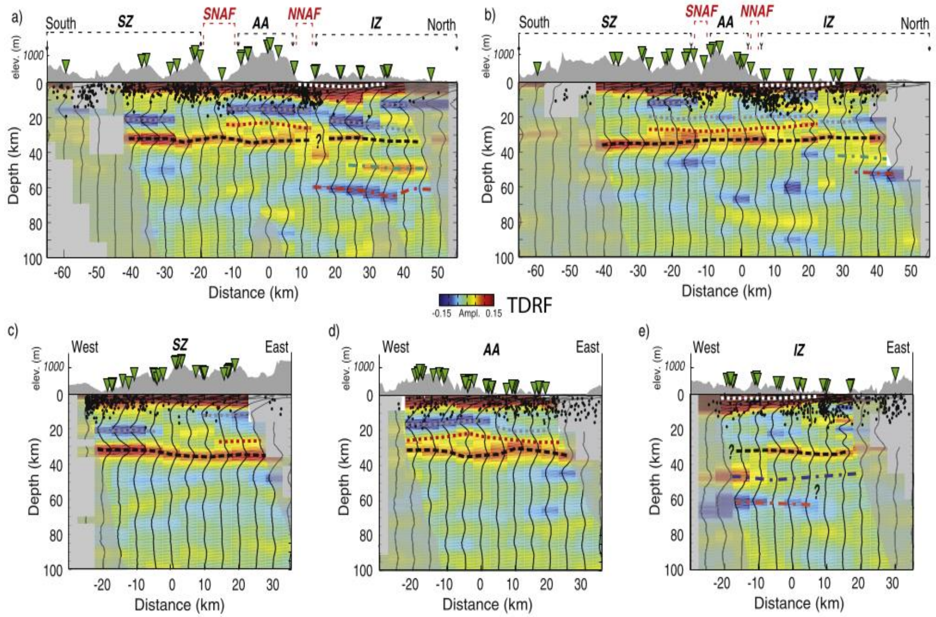

- H-k Stacking and Inversion of RFs with Neighbourhood Algorithm
- Significant lateral variations detected in the upper crust (~10 km).
- Western profile suggests a steeply dipping vertical fault extension for both northern and southern branches.
- NNAFZ can reach into upper mantle, at least 50 km.

Seismic Anisotropy

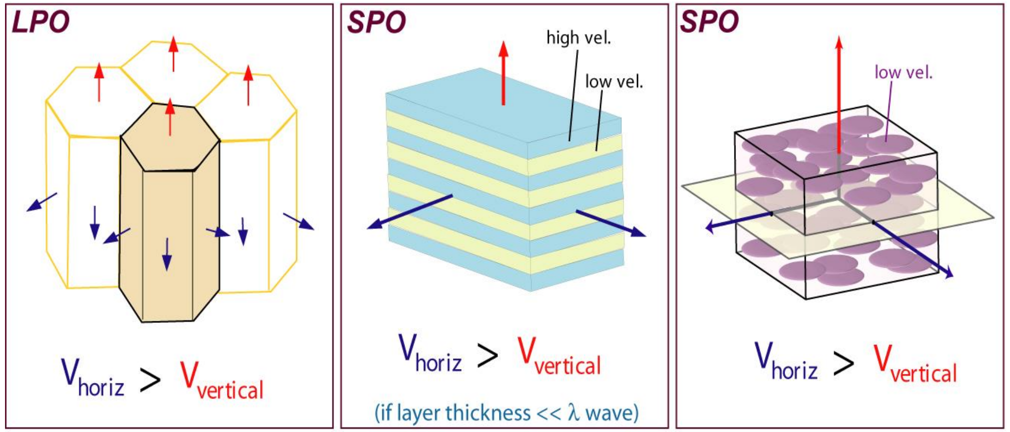

[after Moore,Garnero,Lay,Williams, JGR, 2004]

Lattice Preffered Orientation (SPO) vs. Shape Preffered Orientation (SPO)

- LPO: caused by plastic deformation in the crystal structure and originated from mineral alignment
- SPO: associated with the deformation caused by the faulting, mechanical deformation

- D'' Transition Layer
  - Anisotropy caused by topograhy varition between Core-Mantle Boundary

- Mantle Anisotropy
  - Mostly LPO anisotropy
  - Major factor is variation in temperature
  - Phase differentiation in depth of 410-520-660 km

- Crustal Anisotropy
  - Aligned cracks, foliation in the metamorhic rocks
  - Faults and Volcanic activity

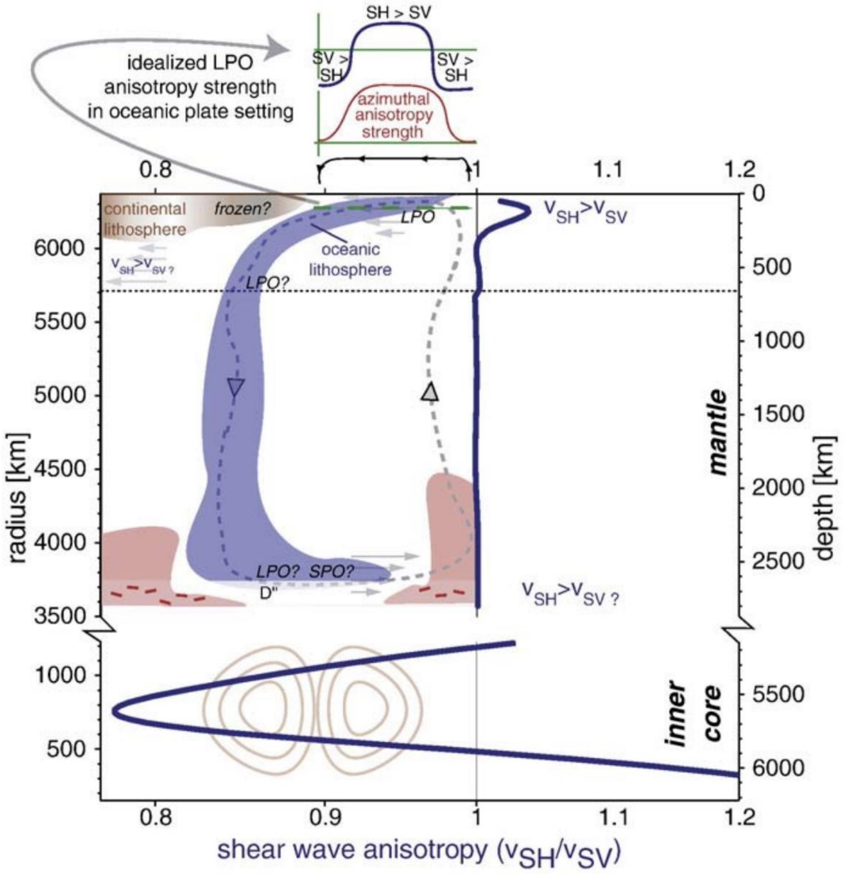

(Long and Becker, 2006)

Methodology: P-Receiver Functions

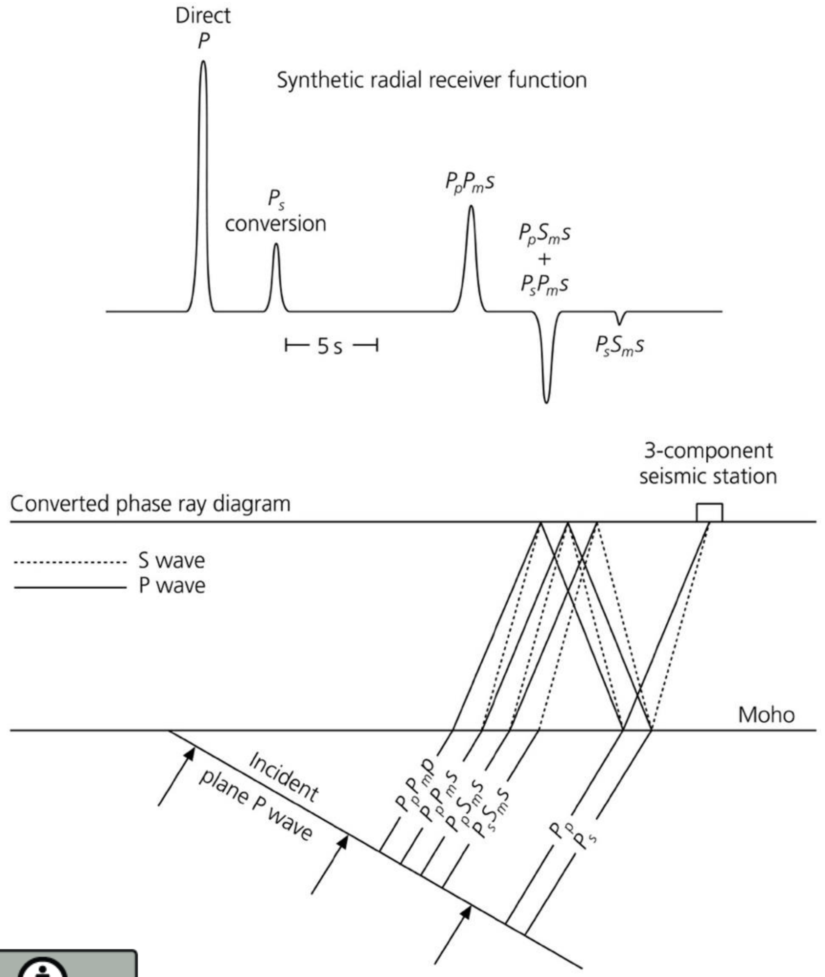

(Stein and Wysession, 2003)

$$H(w) = \frac{S(w)R(w)}{S(w)Z(w)} = \frac{R(w)}{Z(w)}$$

H(w): FT of the receiver function
S(w) : FT of the source signal
R(w) : FT of the radial component of earthquake
Z(w) : FT of the vertical component of earthquake

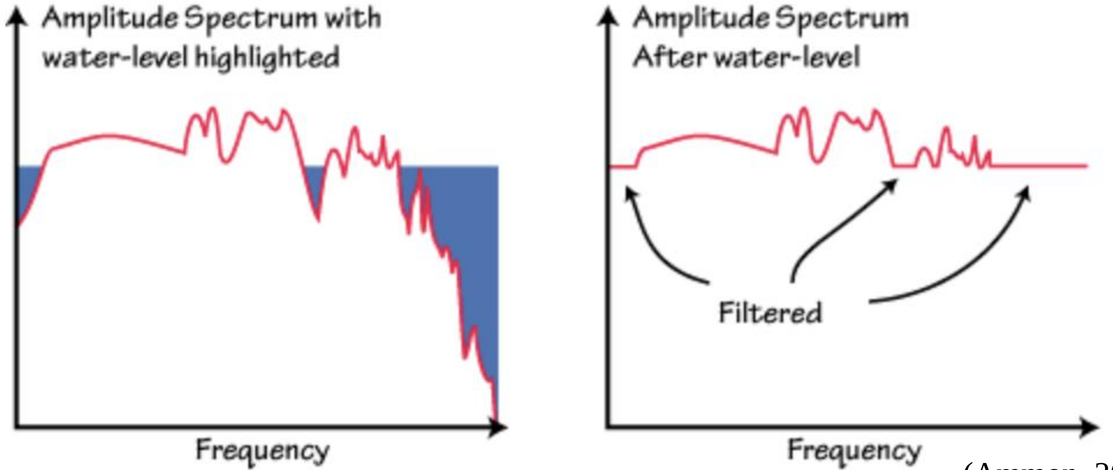

(Ammon, 2006)

Water-Level Deconvolution

- Useful for avoiding division operation using very small numbers in the denominator parameter
- Trial and error to choose the wl parameter
- Waterlevel parameter can function as high-pass, low pass and notch filter.

Methodology: Harmonic Decomposition*

Back Azimuthal angle

RRFs

$$
\begin{bmatrix} R_1(t) \\ \cdots \\ R_N(t) \\ T_1(t) \\ \cdots \\ T_N(t) \end{bmatrix} =
\begin{bmatrix}
1 & \cos(\phi_1) & \sin(\phi_1) & \cos(2\phi_1) & \sin(2\phi_1) \\
\cdots & & & & \\
1 & \cos(\phi_N) & \sin(\phi_N) & \cos(2\phi_N) & \sin2(\phi_N) \\
0 & \cos(\phi_1 + \pi/2) & \sin(\phi_1 + \pi/2) & \cos(2(\phi_1 + \pi/4)) & \sin(2(\phi_1 + \pi/4)) \\
\cdots & & & & \\
0 & \cos(\phi_N + \pi/2) & \sin(\phi_N + \pi/2) & \cos(2(\phi_N + \pi/4)) & \sin(2(\phi_N + \pi/4))
\end{bmatrix}
\begin{bmatrix} A(t) \\ B(t) \\ C(t) \\ D(t) \\ E(t) \end{bmatrix}
$$

TRFs

$A(t)$ → k=0

$B(t)$, $C(t)$ → k=1

$D(t)$, $E(t)$ → k=2

*Shiomi & Park (2008), Bianchi et al., (2010), Audet (2015)

- k=0 : It provides to information about isotropic medium. Just having radial receiver functions.
- k=1 : It has **2π** periodicity – **plunging/dipping symmetry axis anisotropy**
- k=2 : It has **4π** periodicity – **horizontal symmetry axis anisotropy**

$$E_{k=1} = [(B_M(i)^2 + C_M(i)^2) - [(B_U(i)^2 + C_U(i)^2)]$$
$$E_{k=2} = [(D_M(i)^2 + E_M(i)^2) - [(D_U(i)^2 + E_U(i)^2)]$$

→ Calculation of energy from k=1 and k=2 harmonics, respectively

(Licciardi et al., 2018)

- If **$E_{k=1}$ > $E_{k=2}$**, the dominant anisotropy is caused by the dipping layers or any mineral or structure which has plunging axis symmetry
- If **$E_{k=1}$ < $E_{k=2}$**, the anisotropy is originated from layering which has the horizontal symmetry axis.

Synthetic Tests

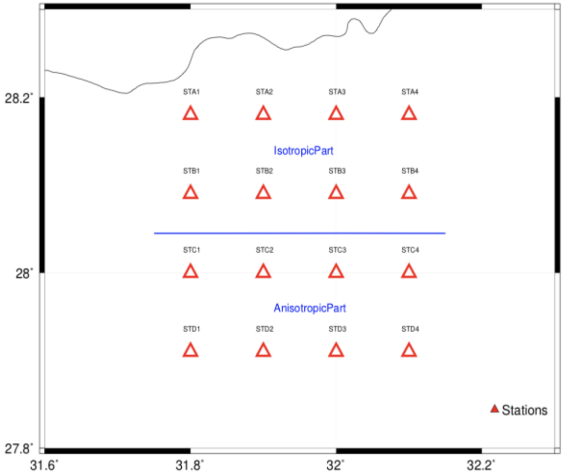

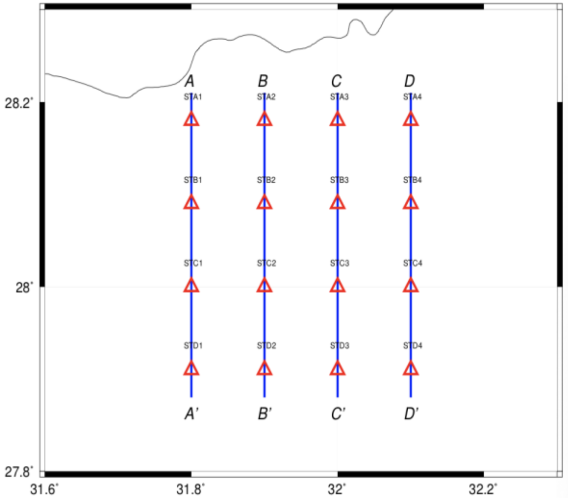

Thickness (km)	ρ (kg/cm³)	Vp (km/s)	Vs (km/s)	%P	%S	trend	plunge	strike	dip
2	2.6	4	2	0	0	0	0	0	0
8	2.89	5.3	3.06	0	0	0	0	0	0
10	2.89	5.3	3.06	20	20	110	45	0	0
15	2.89	5.3	3.06	0	0	0	0	0	0
Half-space	3.15	7.3	4.22	0	0	0	0	0	0

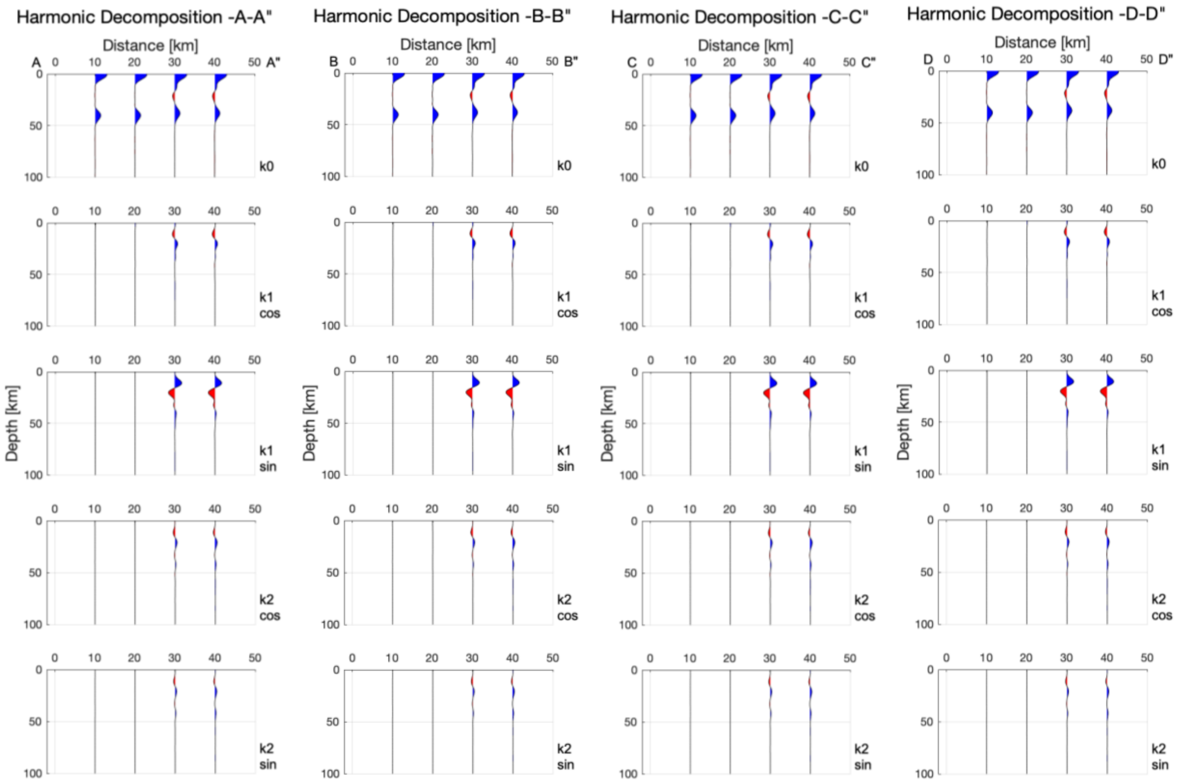

(Keleş et al., *in prep.*)

- Synthetic waveforms are produced by RaySUM (Frederiksen and Bostock, 2000)
- Receiver Functions are calculated by FuncLab software written by Rob Porrit
- 0.02 – 1 Hz Bandpass filtering
- A=2, C=0.01
- Taper=%5

Synthetic Tests

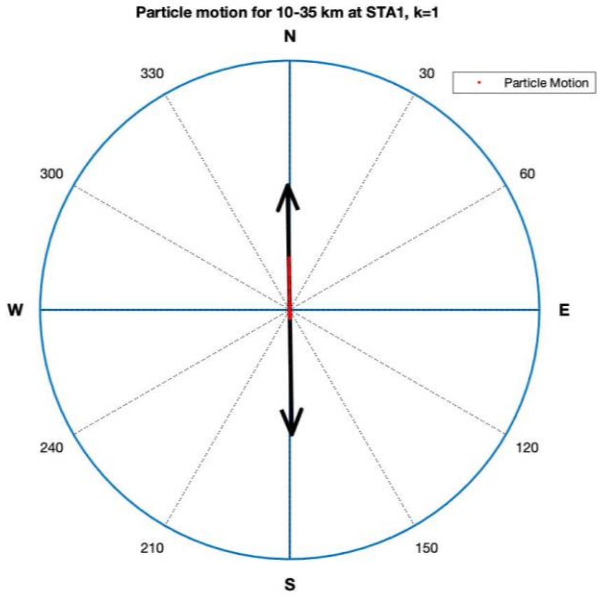

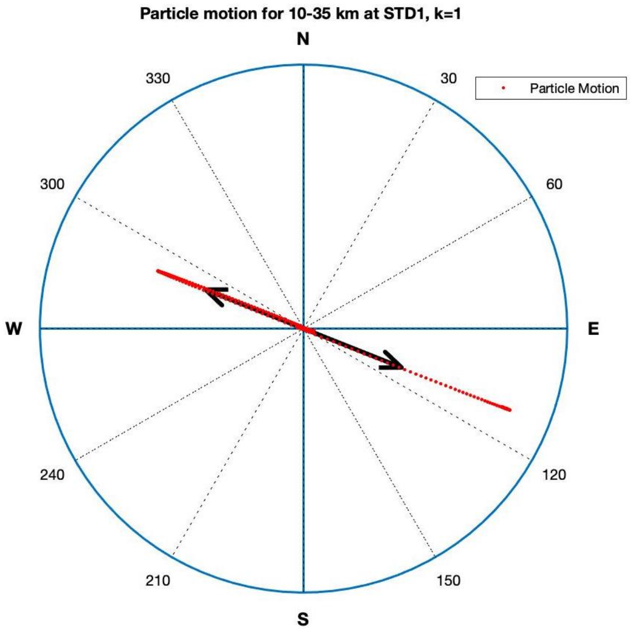

(Keleş et al., *in prep.*)

Results: Real Data Processing

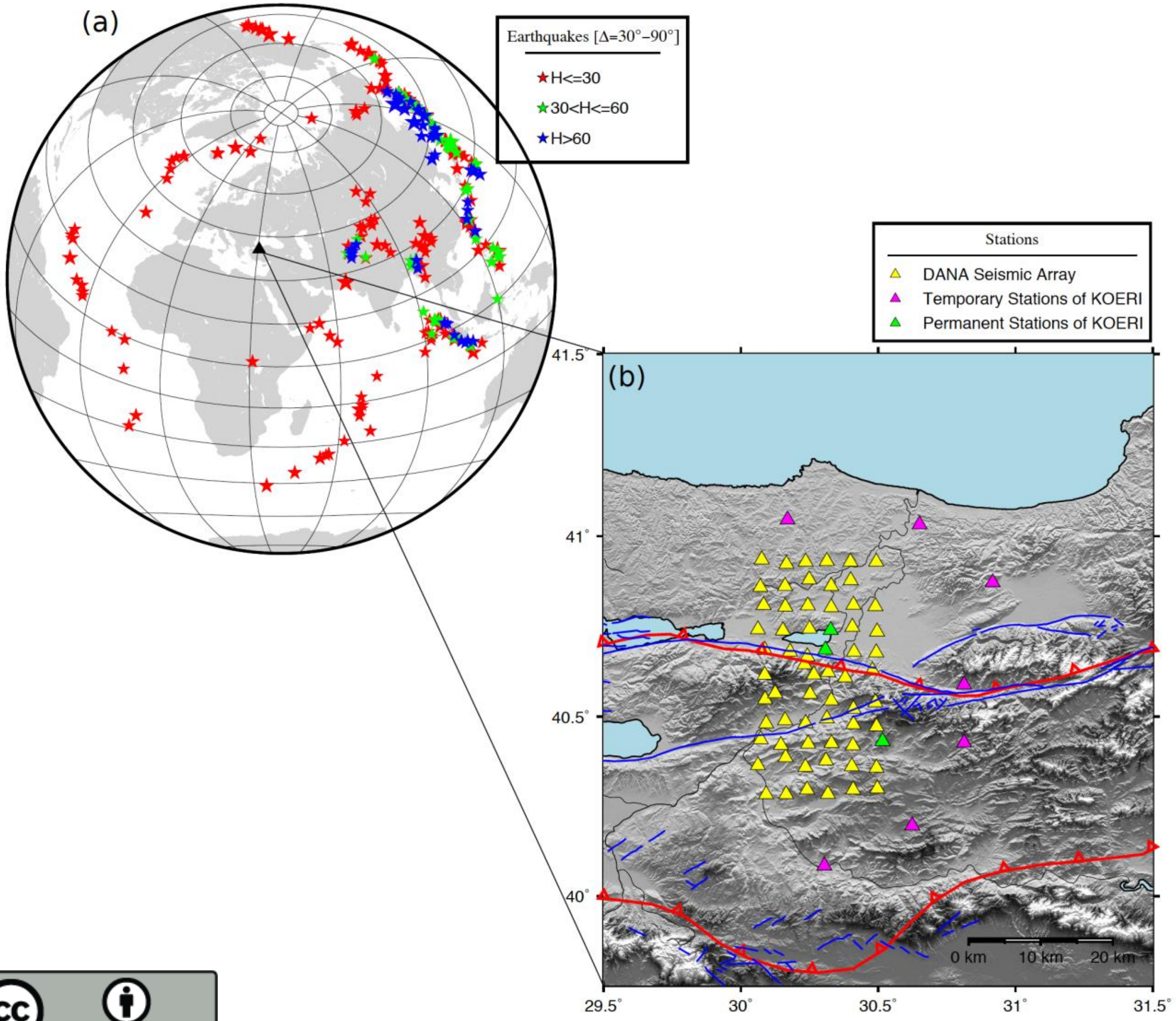

(Keleş et al., *in prep.*)

- 12758 good quality waveforms extracted from 641 teleseismic events
- Epicentral distances and event magnitudes ranging between 30° and 90° and between 5.2 and 8.5, respectively.
- 200 s analysis windows starting 20 s prior to the theoretical P-wave onset.
- Bandpass filtering between 0.02 – 1.25 Hz.
- a=2.2, c=0.01
- Taper= %5

Results

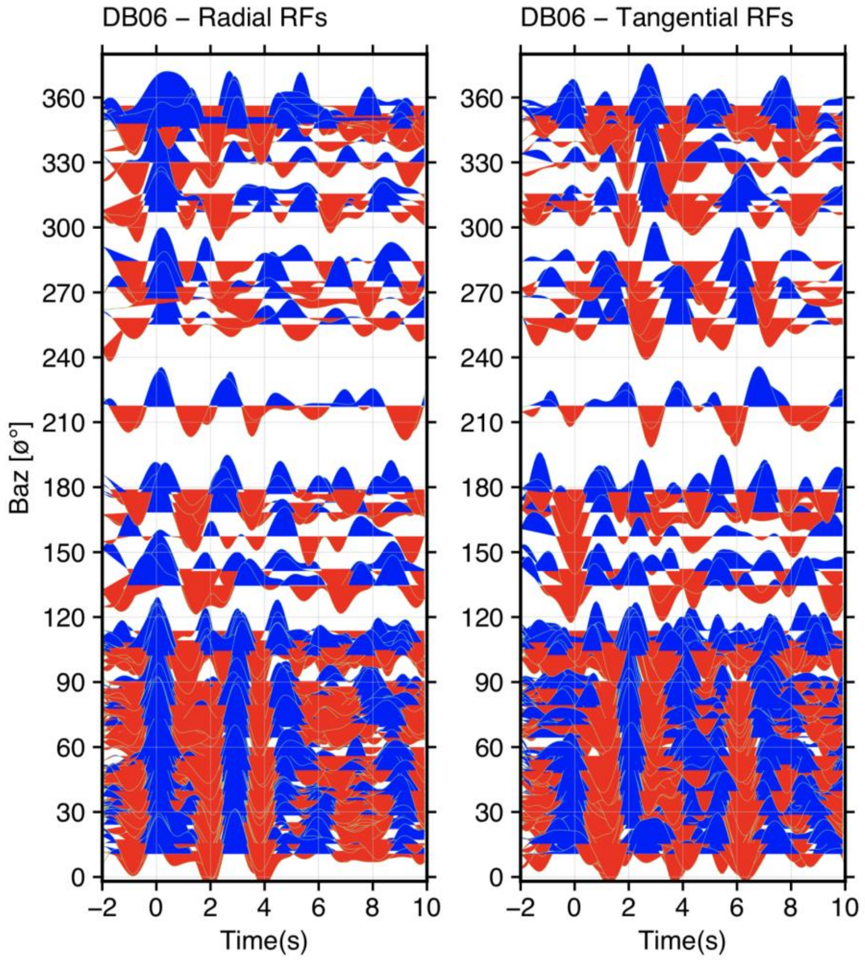

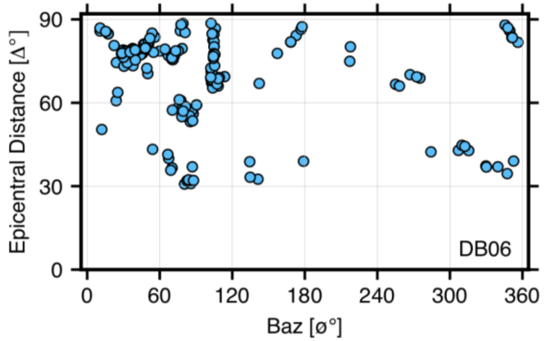

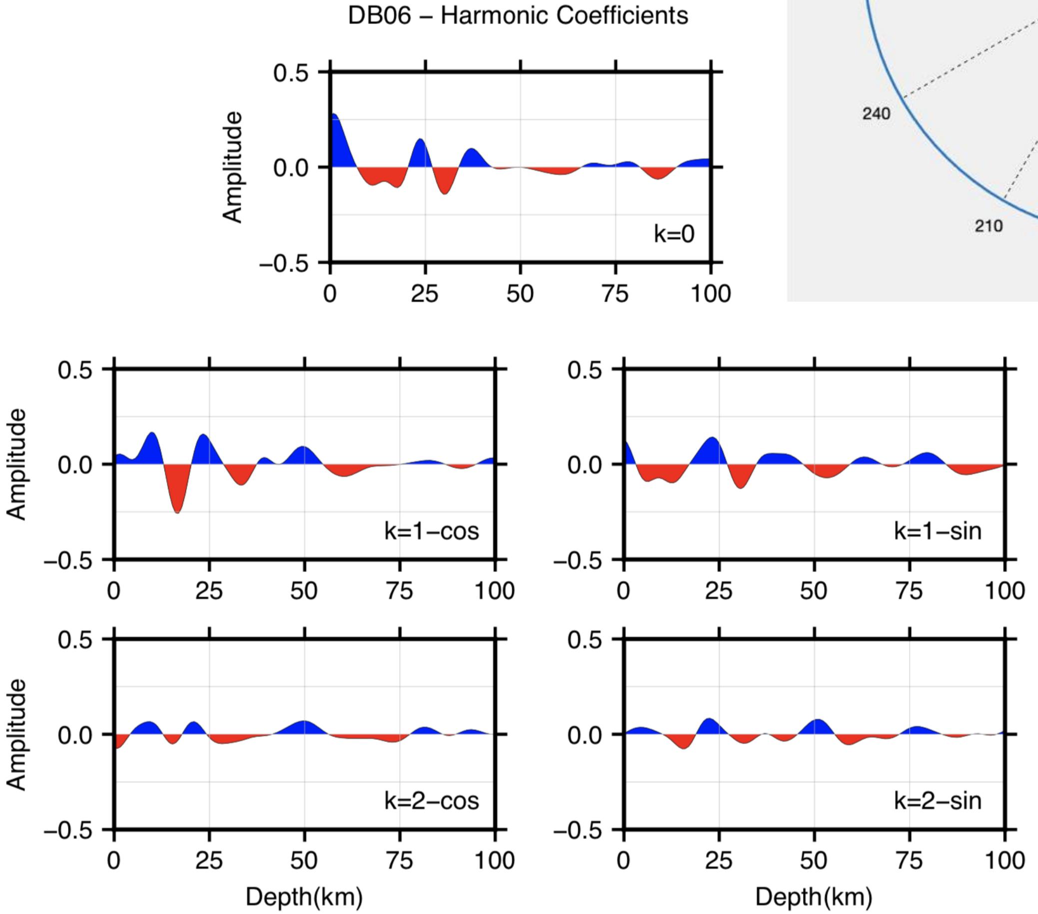

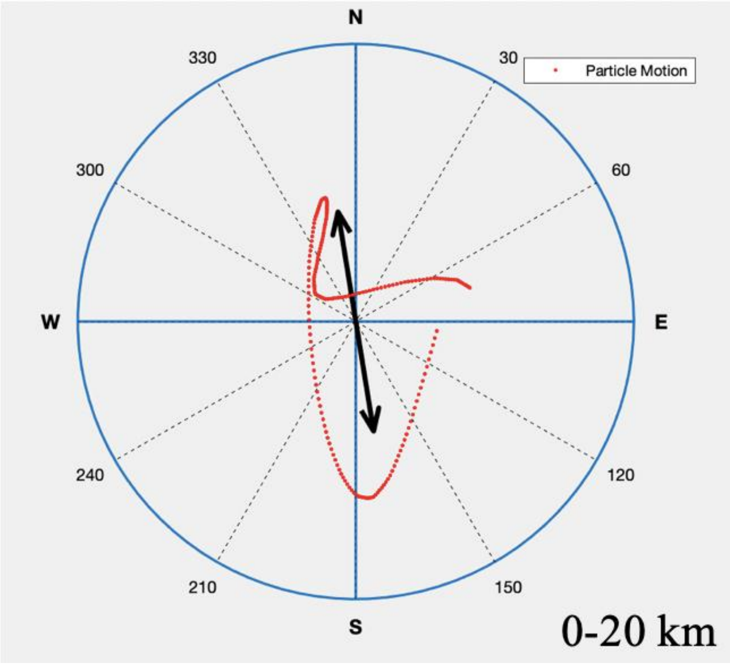

(Keleş et al., *in prep.*)

Discussion and Conclusion

- We implemented the harmonic decomposition method inferred from receiver functions on both the synthetic dataset and real dataset.
- Synthetic tests could recover the true model, which is used to generate synthetic waveform.
- The initial results from real data analyses suggest that the Moho is relatively thick beneath the northern part.
- Beneath the DB06 station, anisotropic orientation shows the approximately N-S direction for the upper crustal part.

Further Processes

- Complete mapping the symmetry axis of anisotropy and energy distribution using k=1,2 harmonics for all depth ranges.
- SKS splitting measurements to understand the crust-mantle interaction.
- Implementing the RFs inversion using *a priori* constraints from the harmonic decomposition results.

References

- **Akbayram, K., Sorlien, C. C. & Okay A. I. (2016).** Evidence for a minimum 52 ± 1 km of total offset along the northern branch of the North Anatolian Fault in northwest Turkey. Tectonophysics, 35(41), 668–669. http://dx.doi.org/10.1016/j.tecto.2015.11.026 0040-1951
- **Ammon, C. J. (2006).** An Overview of Receiver-Function Analysis. Webpage. Department of Geosciences Pennsylvania State University. Available from: http://eqseis.geosc.psu.edu/~cammon/HTML/RftnDocs/rftn01.html.
- **Audet, P. (2015)**. Journal of Geophysical Research : Solid Earth Layered crustal anisotropy around the San Andreas Fault near Parkfield , California. *Journal of Geophysical Research: Solid Earth*, *120*(May), 1–17. https://doi.org/10.1002/2014JB011821
- **Bianchi, I., Park, J., Piana Agostinetti, N., & Levin, V. (2010).** Mapping seismic anisotropy using harmonic decomposition of receiver functions: An application to Northern Apennines, Italy. *Journal of Geophysical Research: Solid Earth*, *115*(12), 1–14. https://doi.org/10.1029/2009JB007061.
- **Frederiksen, A. W. & Bostock, M. G. (2000).** Modelling teleseismic wave in dipping anisotropic structures. Geophys. J. Int. 141, 401-412. https://doi.org/10.1046/j.1365-246x.2000.00090.
- **Frederiksen, A.W., Thompson, D.A., Rost, S., Cornwell, D.G., Gülen, L., Houseman, G.A., Kahraman, M., Poyraz, S.A., Teoman, U.M., Türkelli, N. & Utkucu, M. (2015).** Crustal thickness variations and isostatic disequilibrium across the North Anatolian Fault, western Turkey. Geophys. Res. Lett. 42. doi:10.1002/2014GL062401
- **Kahraman, M., Cornwell, D. G., Thompson, D. A., Rost, S., Houseman, G. A., Türkelli, N., et al. (2015).** Crustal-scale shear zones and heterogeneous structure beneath the North Anatolian Fault Zone, Turkey, revealed by a high-density seismometer array. Earth and Planetary Science Letters, 430, 129–139.
- **Licciardi, A., Eken, T., Taymaz, T., Piana-Agostinetti, N. & Yolsal-Çevikbilen, S. (2018).** Seismic anisotropy in central north Anatolian Fault Zone and its implications on crustal deformation. Physics of the Earth and Planetary Interiors, 277, 99–112.
- **Long, M. D., & Becker, T. W. (2010).** Mantle dynamics and seismic anisotropy. *Earth and Planetary Science Letters*, *297*(3–4), 341–354. https://doi.org/10.1016/j.epsl.2010.06.036.
- **Shiomi, K., & Park, J. (2008).** Structural features of the subducting slab beneath the Kii Peninsula, central Japan: Seismic evidence of slab segmentation, dehydration, and anisotropy. *Journal of Geophysical Research: Solid Earth*, *113*(10), 1–13. https://doi.org/10.1029/2007JB005535
- **Stein, S., & Wysession, M. (2003).** An Introduction to Seismology, Earthquakes and Earth Structure. *Blackwell Publishing,* Oxford, UK. ISBN-13: 978-0-86542-078-6.
- **Porritt, R. W. and Miller, M. S.,(2018).** Updates to FuncLab, a Matlab based GUI for handling receiver functions. Computers and Geoscience, 111, 260-271, doi:10.1016/j.cageo.2017.11.022
- **Taylor, G., Rost, S., Houseman, G. A. & Hillers G. (2019).** Near-surface structure of the North Anatolian Fault zone from Rayleigh and Love wave tomography using ambient seismic noise. Solid Earth, 10, 363-378. https://doi.org/10.5194/se-10-363-2019.